Phys. Status Solidi A **208**, No. 6, 1270–1274 (2011) / **DOI** 10.1002/pssa.201001212

physica status solidi a
www.pss-a.com
applications and materials science

Anodic repassivation of low energy Au-implanted ultra-thin anodic Al_2O_3

Andrei Ionut Mardare[1], Alexander Melnikov[2], Andreas Dirk Wieck[2], and Achim Walter Hassel[*,1]

[1] Institute for Chemical Technology of Inorganic Materials, Johannes Kepler University, 4040 Linz, Austria
[2] Chair of Applied Solid State Physics, Ruhr-Universität Bochum, 44780 Bochum, Germany

Received 10 November 2010, revised 8 March 2011, accepted 9 March 2011
Published online 18 May 2011

Keywords anodic oxide film, ion implantation, scanning droplet cell

[*] Corresponding author: e-mail hassel@elchem.de, Fax: +43-732-2468-8905

Ultrathin anodic alumina with a film thickness of 11 nm was implanted by Au atoms with low energy of 2, 5 or 10 keV. Stopping range simulations yielded three essentially different geometries ranging from surface near implantation over well penetrated oxide to near oxide metal interface implantation, covering the entire range of possible implantation modifications. This work aims at demonstrating how to perform band gap engineering in alumina not only on an energetic level but also targeting a certain geometrical position of the doping atoms by means of the implantation parameters. Beside the intended implantation the oxide destruction in the implantation path and its possible repair was of interest. The repassivation behaviour was considerably different showing a significant redox contribution of the gold nanoclusters on top of the simple oxide repassivation. Near surface implanted Au remained electrochemically active for low repassivation potentials. Higher repassivation potentials always buried the implanted Au atoms under anodic alumina. The repassivation charge determined allowed determining the volume destructed by the implantation.

1 Introduction Band gap engineering is a fashionable approach in semiconductor research. Little has been contributed for the design of nearly insulating, large band gap materials such as alumina. This is a bit surprising since the effects that can be achieved are manyfold and large for those systems. The present works aims at showing a way on how to place centres for resonant tunnelling at a certain position into the band gap, not only on the energetic level but also geometrically between the adjacent conducting phases that may serve as source and drain for transported electrons. A promising method seems to be ion implantation which has gained a good reputation during the last two decades as an attractive method for modifying the near-surface properties of oxides [1]. High energy (MeV) Au implantation in SiO_2 can lead to formation of nanoparticles with shapes and sizes strongly affected by the subsequent thermal annealing [2]. Ultramicrohardness studies of Al_2O_3 modified by various ions implanted at high energies have shown a general increase in the hardness of the oxide even though the outer most surface became softer after Au implantation [3]. Many studies have been conducted regarding the implantation of various ions in Al_2O_3 [4–8] and recent studies have shown that Au nanoparticles can be synthesized under the surface of Au implanted oxide substrate if enough energy is provided, e.g. by means of thermal treatments [9]. Crystalline α-Al_2O_3 was employed for all these studies. Dielectric breakdown measurements on aluminium oxide have shown that the maximum breakdown film strength is equal to the formation field strength under stationary corrosion conditions [10]. This value is typically not reached by crystalline oxide films indicating the existence of weak paths in the oxide. Films grown under potentiostatic conditions or potentiodynamically are tougher and can reach the theoretical breakdown strength [11]. Electrical annealing under initiated and halted breakdown conditions may even lead to a stability exceeding this value but is not considered here [12]. In this work, the low energy implantation of Au in amorphous anodically grown Al_2O_3 and the electrochemically induced Au nanoparticle synthesis at room temperature are studied. The idea behind this work is both of academic interest to better understand the interaction of implanting ions with the substrate and of technical relevance for tailoring dielectric materials with tiny – nanometer sized structural elements located in the band gap of the dielectric material. They would not simply act as doping atoms but may act in a more complex way. They may serve as centres for resonance

tunnelling or allow creating a coulomb blockade; both can be interesting for band gap engineering. The band gap formed by a thin layer of an insulating material is not only confined by the valence band edge and the conduction band edge on the energetic scale but also geometrically by the adjacent conducting phases, namely the parent metal aluminium and the electrolyte. The implantation depth directly addresses the geometrical position within the band gap, whereas the position on the energetic scale may be further influenced by the conditions of the subsequent anodization.

2 Experimental Aluminium thin films were deposited at room temperature on 15 mm × 15 mm × 0.3 mm amorphous silica substrates (Marienfeld microscope cover glasses) from 99.9995% purity Al foils (Alfa Aesar) using the electron beam evaporation technique. The target material was compressed in a tungsten crucible. The vacuum system had a base pressure of 1×10^{-4} Pa and the thickness of the films was monitored *in situ* using a quartz crystal microbalance in order to obtain 300 nm thick films. Before each deposition, the SiO_2 substrates were cleaned using isopropanol (p.a. quality) and high purity de-ionized water. In order to ensure high quality films, evaporation rates as low as 1 nm s^{-1} were used.

3 Results and discussion The Al thin films were locally anodized in acetate buffer electrolyte (pH 6.0) using a scanning droplet cell (SDC) with a tip diameter of 200 μm [13]. The reference electrode (RE) used was a self-made μ-AuHg/$Hg_2(CH_3COO)_2$/$Na(CH_3COO)$ capillary reference electrode [14] with a tip diameter of 100 μm. A gold band (99.999% Wieland Dentaltechnik, Germany) wrapped around the RE served as counter electrode (CE). The glass capillary containing the RE provided electrical insulation towards the CE. After the electrolyte contact with the Al surface, the tip of the SDC was moved in circular patterns using a 3D scanner [15] for wetting a region of approximately 1 mm in diameter before oxide growth. Circular spots of anodic Al_2O_3 were then grown using potentiostatic anodization at 5 V for 200 s, so that ultra-thin layers with a total thickness of 10.6 nm of Al_2O_3 were obtained. The thickness achieved can be directly calculated using the film formation of 1.6 nm for aluminium in this buffer [13] and the thermodynamic oxide formation potential [16, 17].

A Canion 31 Plus focused ion beam (FIB) column from Orsay Physics was used for Au implantations in oxide grown anodically on Al thin films. The ion beam accelerating voltage was 30 kV and additional suppression fields between the column and the target were used for decelerating the ions so that low energy implantations were possible [18, 19]. A theoretical study was conducted in order to establish the optimum parameters necessary for implantation of Au ions in a 10 nm thick Al_2O_3 layer. Using the Stopping and Range of Ions in Matter (SRIM) software [20], the penetration depth of the Au ions in Al_2O_3 was calculated for three different implantation energies and the results are summarized in Fig. 1. Assuming a single incidence point on the surface of the oxide, a Gaussian distribution of the implanted ions can be observed. The accuracy of these calculations can decrease in the case of very low ion energies which may yield much deeper penetration than SRIM simulates. The idea in this situation is that if ions have lower energy than the bandgap of the target (only a few eV) there cannot be any electronic stopping any more besides the nuclear stopping. This was first observed in gas targets [21] but was not clearly demonstrated for metals [22].

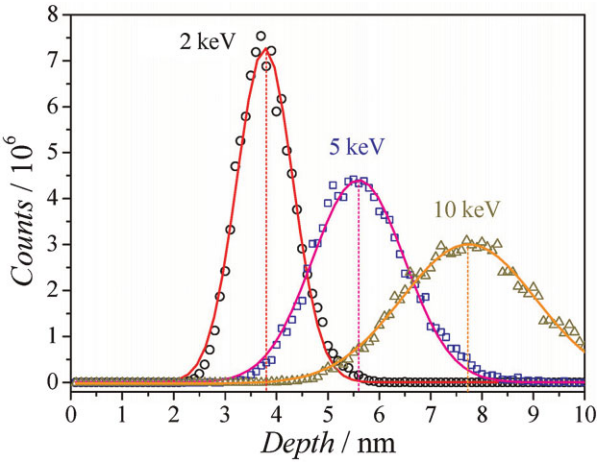

Figure 1 (online colour at: www.pss-a.com) SRIM calculation of the stopping range of Au ions implanted in Al_2O_3 with different energies.

Square surfaces (500 μm × 500 μm) on the anodic Al_2O_3 spots were implanted with Au ions having energies of 2, 5 and 10 keV. The beam diameter was around 100 nm and a relatively high fluence of 1×10^{16} cm^{-2} was necessary for facilitating the study of the electrochemical behaviour of the Au implanted anodic Al_2O_3.

This value depends on the threshold of the 2D–3D transition for Au clusters [23] which led to the observation of Au nanoparticles only for implantation fluences higher than 5×10^{15} cm^{-2}. The average stopping ranges for Au ions are 3.8, 5.6 and 7.7 nm (with associated FWHM values of 1.3, 2.1 and 3.1 nm) corresponding to implantation energies of 2, 5 and 10 keV, respectively. At low implantation energies, e.g. 2 keV, the Au ions fill a well-defined volume inside the oxide as suggested by the sharp depth distribution. When increasing the kinetic energy of the Au ions (10 keV), the volume occupied by the Au inside the oxide starts to be less defined, with an increased probability for scattering due to cascade collisions. In principle, ion channelling may also occur inside the oxide accentuating this effect. On one hand, the ion channelling is generally conditioned by the degree of sample crystallinity and can occur only in vicinal directions in nearly perfect single crystals.

This may not necessarily be the case here, since the anodic alumina is commonly regarded as quasi-amorphous. On the other hand, above fluences of about 10^{15} cm^{-2} amorphization sets in anyway due to the ion bombardment, destroying any possibility of channelling. Nevertheless,

for the 10 keV implantation energy the depth distribution of the ions becomes broader as can be observed in Fig. 1. This leads to a lower volume density of the Au compared with lower ion energies at constant fluence.

The surface microstructure of anodic Al_2O_3 after Au implantation at 2, 5 and 10 keV was analyzed by SEM and the images are shown in Fig. 2a–c, respectively. The formation of uniformly distributed Au clusters with diameters smaller than 10 nm due to the high Au mobility [24] is visible in Fig. 2a for the shallow implantation at 2 keV. The Al grains are also visible, with sizes of approximately 200 nm. Some of these grains, randomly distributed on the surface of the Al film are slightly higher than the rest appearing brighter in the SEM images. Increasing the kinetic energy of the Au ions to 5 keV resulted in a smaller number of observable Au clusters (Fig. 2b) suggesting a dependence of the Au mobility on the ion range in anodic Al_2O_3. This can be explained considering that in the first case of the shallow implants, the Au ions were actually mobile on the surface of the oxide, rather than inside of it due to their calculated stopping range of less than 4 nm. In the case of the Au implantation at 10 keV (Fig. 2c), the preferential formation of small clusters along the Al grain boundaries is observed together with effects of radiation damage in the oxide layer.

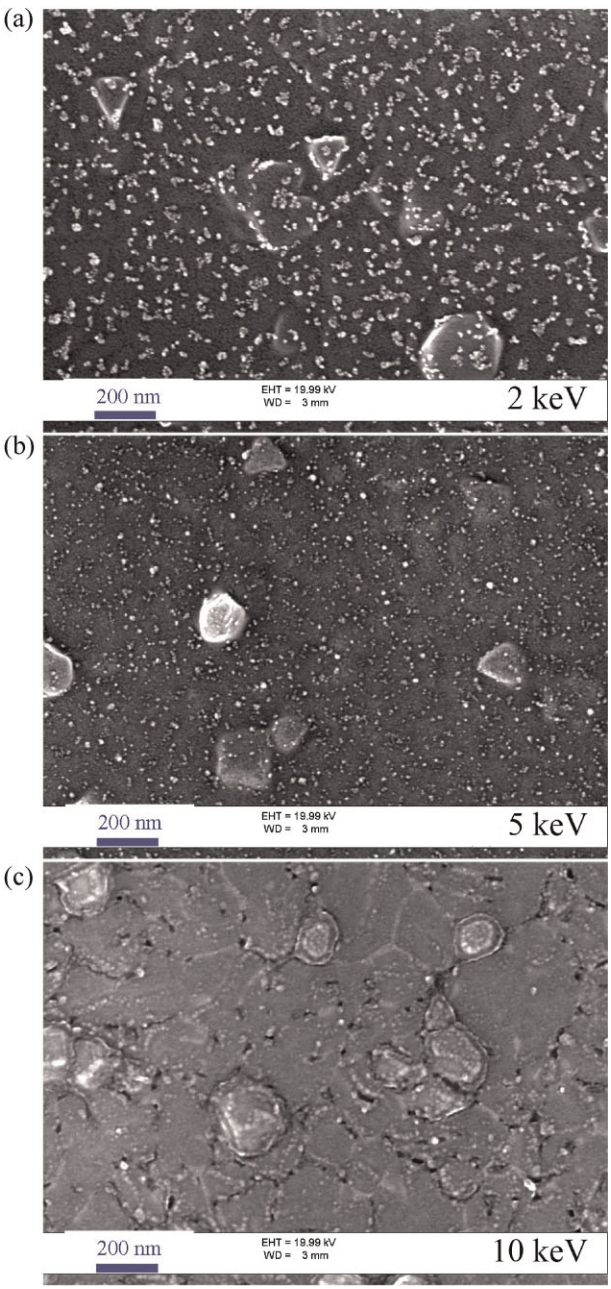

Figure 2 (online colour at: www.pss-a.com) SEM images of Al_2O_3 surfaces immediately after Au implantation at different (a) 2, (b) 5 and (c) 10 keV energies.

The SDC was used for repassivation of the Au implanted areas. A potentiodynamic sweep at a rate of 100 mV s^{-1} was used for this purpose, with the maximum applied potential not exceeding the previous oxide formation potential of 5 V. After the anodic repassivation at 5 V, the same implanted regions presented in Fig. 2 were again imaged by SEM and the results are shown in Fig. 3a–c. Due to the electrochemical treatment, the shallow implant at 2 keV (Fig. 3a) showed a structure reorganization resulting in the formation of Au cluster chains and nanoparticles with diameters of at least 3 times bigger than the Au clusters formed immediately after implantation (Fig. 2a). The same trend is visible for the case of Au implantation at 5 keV (Fig. 3b) where smaller clusters are formed, while a further Au clustering in the anodic oxide implanted at 10 keV (Fig. 3c) was less visible. This can again be related to different Au mobilities as a function of the depth at which they are present in the anodic oxide.

The electrochemical repassivation of the Au implanted regions was achieved in 1 V steps up to the anodic oxide formation potential. The cyclic voltammograms recorded during the electrochemical treatment are shown in Fig. 4 for different Au implantation energies. For all the samples, a repassivation of the anodic oxide was observed, characterized by the presence of current plateaus in the voltammograms due to charge consumption according to Faraday's law $Q = m(zF/M)$, where Q is the total charge, m is the mass, z is the ionization number, F is Faraday's constant and M the molar mass of the oxide.

The repassivation appeared due to the sputtering effect of the Au ions during implantation and is most evident in the case of the highest implantation energy where the current plateaus can be observed for polarizations up to 3 V. In all the samples, during the polarization at 3 V, a sudden current increase characterizing side reactions most likely oxygen evolution can be observed. For the low energy implantations at 2 keV, the presence of the pair of Au oxidation-reduction current peaks was detected during the polarization at 2 V. Smaller peaks indicating redox reactions on Au are also present in the curves recorded during the repassivation of Al_2O_3 implanted at 5 keV, while no Au oxidation could be detected for the high energy implanted spots. The occurring of the redox reactions on Au nanoparticles is somewhat surprising due to the thick underlying Al_2O_3 which is not

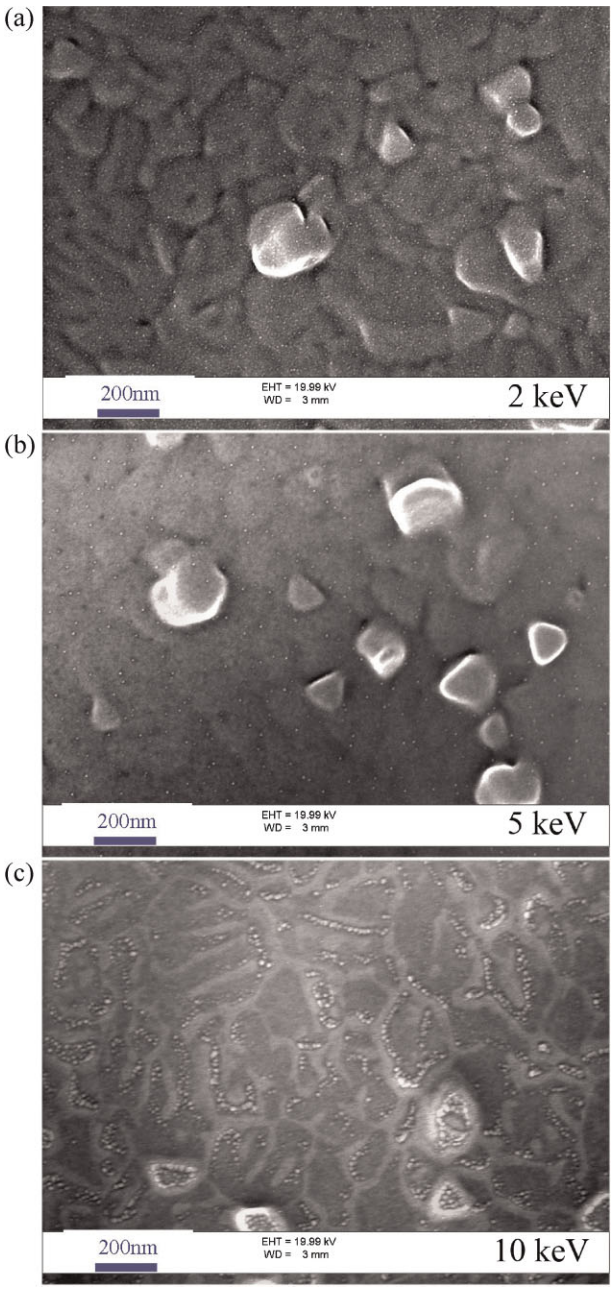

Figure 3 (online colour at: www.pss-a.com) SEM images of Al_2O_3 surfaces immediately after electrochemical repassivation.

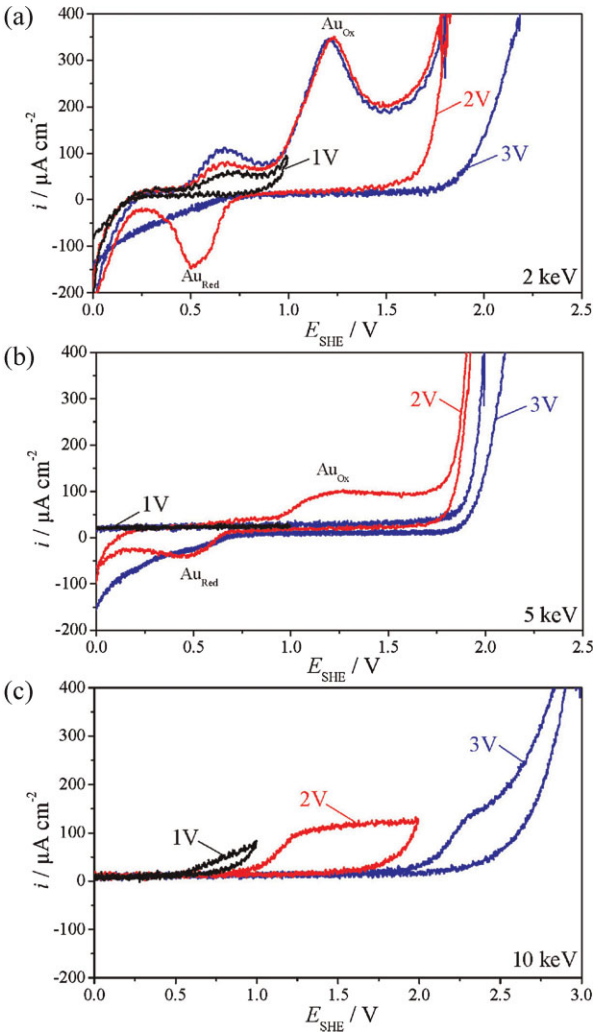

Figure 4 (online colour at: www.pss-a.com) Cyclic voltammograms recorded during repassivation of Au implanted anodic Al_2O_3.

easily tunnelled by electrons coming from the bulk Al (working electrode). A plausible explanation is the existence of small Au clusters within the Al_2O_3 that serve as resonance tunnelling centres providing electrons necessary for the redox reactions to occur.

The curves presented in Fig. 4 can be used for calculating the charge consumed during the repassivation by numerically integrating the current over time (not shown here). Due to the proportionality between the charge and the mass of the re-grown oxide (Faraday's law), one can easily calculate the total sputtered volume of alumina during the Au implantation at different energies by using the alumina density value of 3.5 g cm^{-3}. The sputtered volume during a single implantation event can be further calculated taking into account the area of implantation beam (100 nm in diameter) and the wetted area during the repassivation (200 μm in diameter). These results are presented in Fig. 5 together with a schematic description of the implantation process, where the sputtered volumes of alumina are represented in a conical geometry.

At low implantation energies, such as 2 keV, a smaller sputtered volume is to be expected and a more localized Au deposit, as compared with higher energies. This is also described in Fig. 1. During the repassivation of the 2 keV implanted region, there is a high probability that the tip of the cone will be obstructed by the re-growing alumina on the inner surface, since the vertical oxide growth from bulk will be difficult due to the compact Au deposit. This can be observed directly in Fig. 4 where the reduction peak for Au is missing in the 3 V cyclic voltammogram, suggesting that the cone was

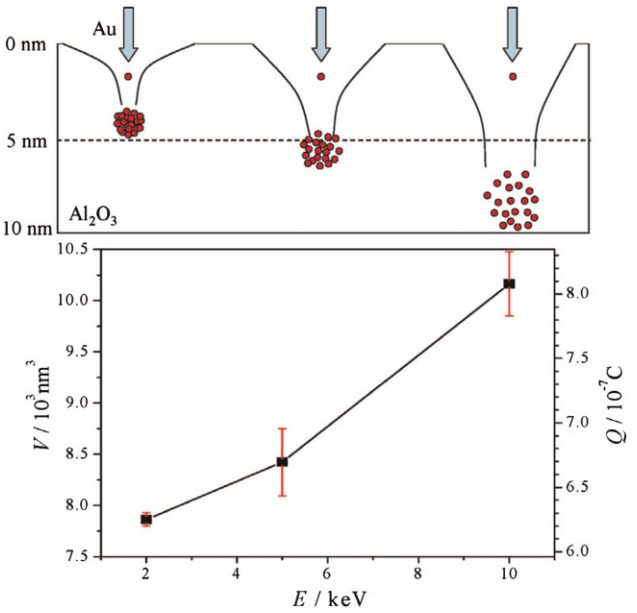

Figure 5 (online colour at: www.pss-a.com) Schematic drawing of the implantation process in alumina and the calculated sputtered volumes versus the ion impact energy.

already obstructed before the Au reduction could take place. Increasing the implantation energies, the sputtered volumes, penetration depths and straggling are also increasing and the repassivation process starts to be observed also vertically from the bulk of the oxide since the in-depth Au distributions are broader. This can be observed in the cyclic voltammograms during the repassivation of the 10 keV implanted region, where Au is not reduced or oxidized anymore. This can be due to trapping of the implanted Au in the re-grown oxide. A similar effect was recently reported during the embedment in the background oxide of Au nanoparticles deposited on the surface of alumina [25].

4 Conclusions Anodic repassivation of implanted alumina was expected to show a quantitative measure of the destructed oxide from coulometric evaluation of the repassivation curves. Cyclic voltammograms allowed separating the initial oxide repassivation from side reactions that could take place on destructed oxide and small Au nanoclusters forming on the surface. The oxidation-reduction of Au can be correlated with the Au clustering presented in Fig. 2 and can be explained using an electron resonance tunneling mechanism rather than a direct electron tunnelling through the anodic Al_2O_3.

Acknowledgements A. I. Mardare acknowledges the International Max-Planck Research School for Surface and Interface Engineering in Advanced Materials (IMPRS SurMat) for financial support through a fellowship. The Max Planck Institute for Iron Research is acknowledged for providing the experimental facility for some steps in substrate preparation.

References

[1] T. Hioki, A. Itoh, M. Ohkubo, S. Noda, H. Doi, J. Kawamoto, and O. Kamigaito, J. Mater. Sci. **21**, 1321 (1986).
[2] Z. N. Dai, S. Yamamoto, K. Narumi, A. Miyashita, and H. Naramoto, Nucl. Instrum. Methods B **149**, 108 (1999).
[3] M. Ikeyama, T. Tanaka, A. Chayahara, R. A. Clissold, L. S. Wielunski, and M. V. Swain, Nucl. Instrum. Methods B **121**, 335 (1997).
[4] H. Naramoto, C. W. White, J. M. Williams, C. J. McHargue, O. W. Holland, M. M. Abraham, and B. R. Appleton, J. Appl. Phys. **54**, 683 (1983).
[5] C. J. McHargue and C. S. Yust, J. Am. Ceram. Soc. **67**, 117 (1984).
[6] T. Hioki, A. Itoh, S. Noda, H. Doi, J. Kawamoto, and O. Kamigaito, J. Mater. Sci. Lett. **3**, 1099 (1984).
[7] P. J. Burnett and T. F. Page, J. Mater. Sci. **19**, 3524 (1984).
[8] T. Hioki, A. Itoh, S. Noda, H. Doi, J. Kawamoto, and O. Kamigaito, Nucl. Instrum. Methods B **7/8**, 521 (1985).
[9] A. L. Stepanov, C. Marques, E. Alves, R. C. da Silva, M. R. Silva, R. A. Ganeev, A. I. Ryasnyansky, and T. Usmanov, Tech. Phys. **51**, 1474 (2006).
[10] A. W. Hassel and M. M. Lohrengel, Mater. Sci. Forum **185**, 581 (1995).
[11] A. W. Hassel and D. Diesing, Thin Solid Films **414**, 296 (2002).
[12] A. W. Hassel and D. Diesing, Electrochem. Commun. **4**, 1 (2002).
[13] A. W. Hassel and M. M. Lohrengel, Electrochim. Acta **42**, 3327 (1997).
[14] K. A. Lill and A. W. Hassel, J. Solid State Electrochem. **10**, 941 (2006).
[15] A. I. Mardare, A. D. Wieck, and A. W. Hassel, Electrochim. Acta **52**, 7865 (2007).
[16] M. Pourbaix, Atlas of Electrochemical Equilibria in Aqueous Solutions (National Association of Corrosion Engineers, Houston, Texas, USA, 1974), p. 168.
[17] A. I. Mardare, A. P. Yadav, A. D. Wieck, M. Stratmann, and A. W. Hassel, Sci. Technol. Adv. Mater. **9**, 035009 (2008).
[18] M. Mehta, D. Reuter, A. Melnikov, A. D. Wieck, and A. Remhof, Appl. Phys. Lett. **91**, 123108 (2007).
[19] M. Mehta, D. Reuter, A. D. Wieck, S. Michaelis de Vasconcellos, A. Zrenner, and C. Meier, Appl. Phys. Lett. **97**, 143101 (2010).
[20] J. Ziegler, The stopping and range of ions in matter, www.srim.org (2008).
[21] H. J. Assenbaum, K. Langanke, and C. Rolfs, Z. Physik A **327**, 461 (1987).
[22] A. Huke, K. Czerski, and P. Heidea, Nucl. Phys. A **719**, C279 (2003).
[23] M. P. Johansson, A. Lechtken, D. Schooss, M. M. Kappes, and F. Furche, Phys. Rev. A **77**, 7 (2008).
[24] F. Furche, R. Ahlrichs, P. Weis, C. Jacob, S. Gilb, T. Bierweiler, and M. M. Kappes, J. Chem. Phys. **117**, 6982 (2002).
[25] A. I. Mardare, S. Borodin, A. D. Wieck, M. Rohwerder, and A. W. Hassel, J. Phys. Chem. C **113**, 3105 (2009).

